On the two-dimensional numerical modelling of thermal processes in Czochralski crystal growth from melt

by

SONIA S. TABACOVA[1]

Laboratory for Applications
of Mathematics, B A S
15 Vaptzarov Str.
4000 Plovdiv, BULGARIA

A stationary two-dimensional heat conduction dominated mathematical model of the thermo-capillary processes in Czochralski crystal growth is developed. On its basis, an optimization problem is formulated. The crucible and the ambient temperatures are used as control parameters. A cost functional depending on the control vector is assumed in the quadratic form. Constant crystal radius condition is taken as an additional constraint. An optimal solution and constraint set propagation for different discrete melt volumes are determined. Numerical experiments were performed for gallium arsenide and germanium crystals as test materials.

---

[1] Present adress: VMEI "Lenin", Department of Mechanics, 23 Ivan Vazov Str., 4000 Plovdiv, BULGARIA

1. Introduction

The Czochralski technique is one of the most popular methods for the growth of high temperature semiconductor monocrystals of large and medium diameters and good microstructure (distribution of impurities, inner stresses, etc.).

A cylindrical crucible filled with molten semiconductor material is slowly rotated and lifted, while at the same time a vertical rod is rotated and slowly pulled upwards in such a way that its lower end, equipped with crystal seed, continuously touches the melt surface. An appropriate heating of the crucible creates necessary conditions for crystallization from the melt and crystal formation around the seed. The latter strongly depends on the position of the melt/solid interface (the phase change surface) and on the melt/gas interface (the meniscus formed by the melt touching the crystal walls).

Although the Czochralski crystal growth is a very slow process, it still requires a large gradient of temperature (due to difference between the crucible and ambient). It turns out that the heat transfer mechanism dominates all the changes during the whole process duration, i.e. geometrical change - melt volume fall, solidification, heat conduction, thermal convection, Marangoni convection. It has been observed that the above processes can be distinguished from each other and, for the semiconductor materials studied here, they refer to different time scales. The first two are classified as long-time scale processes, while the other - as short-time scale ones.

The main features of Czochralski process, similar to other phase transition processes, are its instability and irregular development in time, which give rise to dendritic formation, over-stresses in the crystal, non-uniform crystal shape, etc. Better understanding of the process dynamics would not only improve prediction of its evolution, but also would show a way of controlling it. In practice, the main

would show a way of controlling it. In practice, the main
problem, no matter to what extent the process is automatic,
is to choose an appropiate criterion or a · combination of
criteria by which the instabilities could be controlled.
Modern methods use crystal diameter monitoring during the
growth process and feedback control laws - some of the
process parameters such as pulling rate or heater power are
modified when the crystal diameter deviates from its desired
value.

The crystal radius deviatons are caused by melt volume
changes and by the solidification mechanism itself, hence
they are observed in the long-time scale. In turn, `the
crystal ripples are due to the convective and turbulent
fluctuations in heat transfer and can be treated within the
short-time scale [4].

In this paper we propose a strategy for control of the
crystal radius exploiting a steady-state two-dimensional
model within the conduction time scale (when no geometrical
or solidification changes are observed and convection is
ignored). The dynamic control will be performed discretely
for different melt volume values, (some other geometrical
parameters, such as crystal length and three-phase
equilibrium curve, could also be used). The steady-state
model at a fixed melt volume is based on mass and energy
balance laws, with conduction dominating. The model is
formulated over a domain with free boundary (unknown crystal
length, meniscus shape, melt/crystal interface).

Section 2 contains the construction of a mathematical
model of the Czochralski crystal growth in dimensional
form. Various approaches are discussed for different time
scales.

Section 3 contains an enthalpy formulation of the
classical steady-state Stefan problem. An approximation via
smoothing is proposed for the obtained problem.

The equation of capillary statics (determining
meniscus shape) and the energy balance equation with
smoothed coefficients are solved numerically by
finite-difference implicit schemes which are described in

In section 5 an optimization problem is discussed in the stationary case.The crucible temperature and the ambient temperature are taken as control variables. An algorithm is proposed for determining the constraint points and the set consisting of these points is approximated a posteriori. From this approximation, forecasting of the constraint set evolution can be obtained for different melt volumes.

In section 6 results of the numerical experiments for two different semiconductor materials - gallium arsenide and germanium - are discussed.

2. Problem statement

We shall consider a cylindrical crystal of radius b grown from a cylindrical crucible of radius a. The melt volume is $V_O(t)$ and the total mass of the melt and crystal is $M(t) \equiv M_O$. A cylindrical symmetry is adopted further and a cylindrical coordinate system (r', φ', z') is introduced. Because we restrict ourselves to pure materials only, mass transfer effects could be ignored.

Fig. 1 gives a schematic representation of our prototype system where $G_1(t)$ denotes the melt region, $G_2(t)$ - the crystal region, $\Gamma_O(t)$ - melt/crystal interface, $\Gamma_1(t)$ - melt/gas interface, $\Gamma_2(t)$ and $\Gamma_3(t)$ - melt (crucible) boundaries, $\Gamma_4(t)$ and $\Gamma_5(t)$ - crystal walls exposed to the ambient gas, $\Gamma_6(t)$ - symmetry axis. The outer normals to the surfaces are $n_i(t)$ $(i=\overline{0,6})$.

The governing equations of energy balance in both regions are:

$$\rho_i \, c_{pi} \, [\, \frac{\partial \Theta}{\partial t} + (\mathbf{U}. \, \nabla)\Theta \,] = \nabla. \, (\lambda_i \, \nabla\Theta \,) \qquad (2.1)$$

where $i=1,2$ - denote the melt and the crystal, respectively (the notations are given in Appendix).

To the energy balance, Navier-Stokes equation in the Boussinesq approximation and the continuity equation are added for the melt region $G_1(t)$:

$$\frac{\partial U}{\partial t} + (U.\nabla)U = - \frac{\nabla \hat{p}'}{\rho_1} + \nu \nabla^2 U + \beta g(\Theta - \Theta_m) e_z \qquad (2.2)$$

$$\nabla U = 0 \qquad (2.3)$$

At the phase change surface $\Gamma_O(t): z' = H_O'$ (r', t), corresponding to the isotherm

$$\Theta = \Theta_m , \qquad (2.4)$$

the mass and energy balance laws are:

$$\rho_1(U - \frac{\partial H_O'}{\partial t} e_z) \cdot n_O' \Big|_1 = \rho_2(U_p - \frac{\partial H_O'}{\partial t})(n_O' \cdot e_z)\Big|_2 \qquad (2.5)$$

$$\lambda_1(n_O' \cdot \nabla\Theta) \Big|_2^1 = \rho_2 H_f(U_p - \frac{\partial H_O'}{\partial t}) (n_O' \cdot e_z) . \qquad (2.6)$$
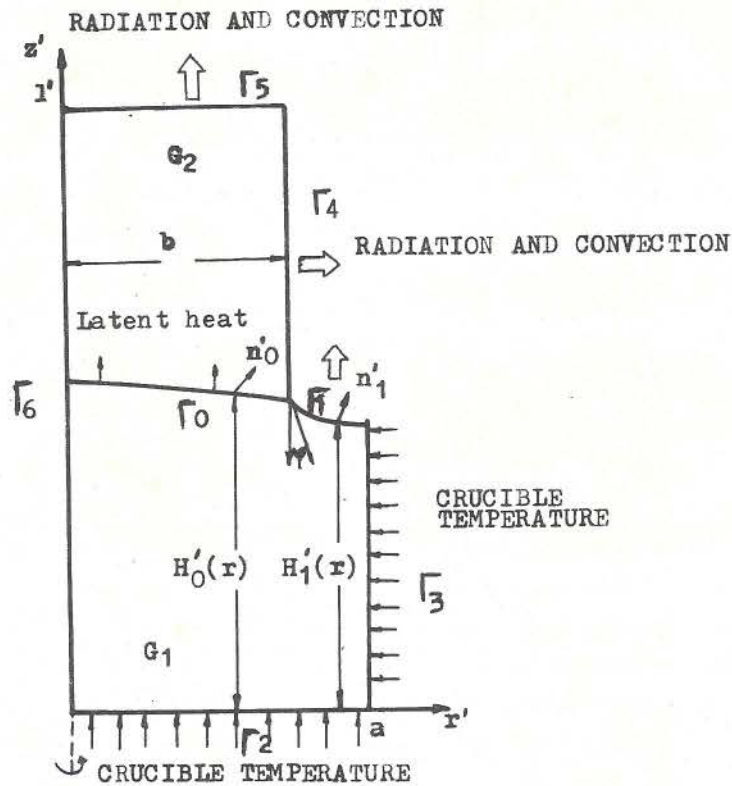
Fig.1. Schematic illustration of Czochralski crystal growth

The axial symmetry at $r'=0$ is expressed as:

$$\frac{\partial \Theta}{\partial r'} = 0 \tag{2.7}$$

Uniform heating is applied to the crucible walls:

$$\Theta = \Theta_{cr} \tag{2.8}$$

Cooling is performed by radiation and convection from the crystal surface and from the melt surface to the ambient gas

$$-\lambda_1(n'_j \cdot \nabla\Theta) = \alpha_j(\Theta-\Theta_a) + \varepsilon_j \sigma(\Theta^4-\Theta_a^4) \tag{2.9}$$

The total length $l'(t)$ of the melt-crystal system is defined from the mass conservation law

$$\rho_1 V_O(t) + 2\Pi\rho_2 \int_O^b (l'-H'_O) r' dr' = M_O \tag{2.10}$$

For our model the equation of capillary statics is sufficient to determine the melt/gas interface $\Gamma_1(t): z'=H'_1(r',t)$,

$$g(\rho_1-\rho_{gas})(H'_1-\gamma') = \sigma_m(\frac{1}{x_1} + \frac{1}{x_2}) \quad \text{on} \quad \Gamma_1(t) \tag{2.11}$$

with

$$\left.\frac{\partial H'_1}{\partial r'}\right|_{r'=b} = \text{ctg } \psi \quad \text{and} \quad \left.\frac{\partial H'_1}{\partial r'}\right|_{r'=a} = 0 \tag{2.12}$$

expressing the meniscus contact with the crystal at the three-phase boundary with a prescribed angle ψ (the change of this angle causes changes in the crystal radius [2] and its perpendicular contact with the crucible wall (in fact this angle is slightly different, but it turns rather difficult to measure it accurately). The unknown reference value γ' is defined from the condition of the melt volume preservation in the crucible

$$\int_{0}^{b} H'_O \; r' \; dr' + \int_{b}^{a} H'_1 \cdot r' \; dr' = V_O(t)/2\Pi \qquad (2.13)$$

The continuity condition

$$H'_1\big|_{r'=b} = H'_O\big|_{r'=b} \qquad (2.14)$$

makes the problem overspecified. However, this does not follow from any physical reason, but is a consequence of our mathematical construction. In order to guarantee uniqueness of the solution, some of the process parameters have to be considered as variables e.g. crystal radius, melt volume, crucible temperature, ambient temperature, etc.

The initial conditions for velocity and temperature are

$$U' (r',z',0)=U'_O (r',z')$$

$$\Theta'(r',z',0)=\Theta'(r', z') \qquad (2.15)$$

where U'_O, $\Theta'_O \in C^2(G(O))$.

As it has been mentioned in introduction, it is convenient to use multiple time scaling. With the following character parameters: a - length, λ_1 - thermal conductivity, Θ_m - temperature, Πa^3 - melt volume, ρ_1 - density, $\rho_1 \, \nu U^*/a$-pressure, t^* - time , U^* - velocity, equations (2.1), (2.2), (2.4), (2.6) in the dimensionless form (the primes being dropped) are:

$$\frac{a}{t^* \, U^*} \cdot [\frac{\partial T}{\partial \tau} + (V.\nabla)\, T] = \frac{\lambda_1}{\rho_1 c_{p1} a U^*} \nabla.(k_1 \nabla T) \text{ in } G_1(\tau) \qquad (2.16)$$

$$\frac{a}{t^* U^*} \cdot \frac{\partial V}{\partial \tau} + (V.\nabla)\; V = - \frac{\nu \nabla \rho}{U^* a} + \frac{\nu}{U^* a} \nabla^2 V + \frac{\beta g a \, \Theta_m}{U^{*2}} (T-1) e_z$$

$$\text{in } G_1(\tau) \qquad (2.17)$$

$$T = 1 \quad \text{ on } \quad \Gamma_O(\tau) \qquad \text{and} \qquad (2.18)$$

$$k_i (n_O \cdot \nabla T)\Big|_2^1 = \frac{\rho_2 H_f a U^*}{\lambda_1 \Theta_m} \left(\frac{U_p}{U^*} - \frac{a}{t^* U^*} \cdot \frac{\partial H_O}{\partial \tau}\right) (n_O \cdot e_z) \quad (2.19)$$

In the geometrical time scale, $t^* = t_g = \frac{a}{U_p} \sim O(10^4 \text{sec})$,

$$U^* = U_p \sim O(10^{-4} \text{cm/sec}), Pe_p = \frac{\rho_i c_{pi} a U_p}{\lambda_1} \ll 1, Re_p = \frac{U_p a}{\nu} \ll 1,$$

$$S = \frac{H_f \rho_2}{c_{pi} \Theta_m \rho_1} \gg 1, Pe_p S \sim O(1) \text{ when neglecting } o(1) \text{ terms,}$$

(2.16), (2.18), (2.19) reduce to:

$$\nabla \cdot (k_i \nabla T) = 0 \qquad\qquad\qquad (2.16')$$

$$k_i (n_O \cdot \nabla T)\Big|_2^1 = Pe_p S \left(1 - \frac{\partial H_O}{\partial \tau}\right) (n_O \cdot e_z) \qquad (2.19')$$

In the solidification time scale, for $t^* = t_s = \frac{a^2 H_f \rho_2}{\lambda_1 \Theta_m} \sim O(t_g)$,

a similar approach is available with a slight difference in the right-hand side of the phase-change condition, which then takes the form $\left(Pe_p S - \frac{\partial H_O}{\partial \tau}\right) (n_O \cdot e_z)$. In such a way, the problem in both time scales remains quasistationary (stationary equations in variable domain $\underset{\tau \in [0,1]}{\cup} G(\tau)$, where

$$G(\tau) = \{\{G_1(\tau) \cup G_2(\tau) \underset{i=0,6}{\cup} (\Gamma_i(\tau))\} : \tau \in [0,1]\} \subset E^3).$$

However, in the conduction time scale,

$$t^* = t_c = \frac{a^2 c_{p1} \rho_1}{\lambda_1} \sim O(10^2 \text{sec}) \text{ and } U^* = U_p, \text{ the charac-}$$

ter non-dimensional numbers are of the same order as in the above case which leads to another form of equations (2.16), (2.19):

$$\frac{\partial T}{\partial \tau} = \nabla \cdot (k_i \nabla T) \tag{2.16''}$$

$$k_i (n_0 \cdot \nabla T)\Big|_2^1 = Pe_p \ S(n_0 \cdot e_z) \quad \text{on} \quad z=H_0 \ (r,\tau) \equiv H_0 \ (r) \tag{2.19''}$$

The last equation follows from (2.19) where $\dfrac{\partial H_0}{\partial \tau} = 0$, due to $S \gg 1$.

So we have come to the fixed-domain case within the conduction time scale ($\bar{G} = G \ (\tau_j)$, where τ_j is any discrete time moment from the long-time scale). If all the data entering equations and boundary conditions are kept fixed during this short time, then with the above restrictions (neglecting all the $O(1)$-terms in equations and in boundary conditions) the temperature distribution satisfying (2.16''), (2.19'') will be stationary and (2.16'') reduces to, [11],

$$\nabla \cdot (k_i \ \nabla \ T) = 0 \tag{2.20}$$

As it is seen from (2.17'), convection has to be treated in the convective time scale, $t^* = t_{cg} = \dfrac{\alpha}{U_{cg}} \sim O(1 \ \text{sec})$, where $U^* = U_{cg} = (\beta g \ a \ \Theta_m)^{1/2} \sim O \ (1 \ \text{cm/sec})$. However, in the limits of the present approach the velocity does not affect the temperature distribution and we are thus not going to take it into account further. Then, we shall try to solve (2.20), (2.19'') together with the remaining boundary conditions (2.7) - (2.14) in dimensionless form:

$$\frac{\partial T}{\partial r} = 0 \qquad \text{on } r = 0 \tag{2.7'}$$

$$T = T_{cr} \qquad \text{on } \Gamma_2 \cup \Gamma_3 \tag{2.8'}$$

$$-k_i (n_j \cdot \nabla T) = Bi_j (T-T_a) + Ra_j (T^4 - T_a^4) \quad \text{on } \Gamma_j, (j=1,4,5) \tag{2.9'}$$

$$\bar{V}_0 + 2\rho_2/\rho_1 \int_O^R (1-H_0)r dr = M_0/\rho_1 \Pi a^3 \tag{2.10'}$$

$$Bo(H_1 - \gamma) = divCH_1 \quad \text{on } \Gamma_1: \; z = H_1(r) \tag{2.11'}$$

where $\quad C = \dfrac{\nabla}{[1 + |\nabla|^2]^{1/2}}$

$$e_r \cdot CH_1 = \cos \psi_i \quad \text{on } \partial\Gamma_1, \; (i = 1, 2) \tag{2.12'}$$

where $\; \psi_1 = \Pi + \psi, \quad \psi_2 = 0 \; , \qquad \partial\Gamma_1 := \{\Gamma_1: \; r = R, \; r = 1\}$

$$\int_O^R H_O r \; dr + \int_R^1 H_1 r \; dr = \bar{V}_O / 2 \tag{2.13'}$$

$$H_1 = H_O \qquad\qquad\quad \text{at } r = R \tag{2.14'}$$

3. Enthalpy formulation of the model

The further treatment of the above classical stationary Stefan problem will be based on its generalized formulation, in terms of the enthalpy function $H(T)$ – discontinuous and multivalued at $T = 1$ [1], [2], [5], [8]:

$$H(T) = \begin{cases} 0 & T < 1 \\ \in [0, 1] & T = 1 \\ 1 & T > 1 \end{cases} \tag{3.1}$$

Then, the temperature function has to satisfy in $\bar{G}$ the equation

$$Pe_p S \, (e_z \cdot \nabla) H = \nabla(k \nabla T) \tag{3.2}$$

where

$$k(T) = \begin{cases} k_2 & T < 1 \\ \in [k_2, k_1] & T = 1 \\ k_1 & T > 1 \end{cases} \tag{3.3}$$

On the singular surface $\Gamma_O: \; z = H_O(r)$ the conservation form of (3.2) yields exactly the boundary conditions (2.19'') and (2.18), while away from Γ_O in the melt and in the crystal region (3.2) coincides with (2.20).

The boundary $\Gamma = \bigcup_{i=1,6} \Gamma i$ is Lipschitz continuous almost everywhere, except at the three-phase point $(R, H_1(r))$ where the outer normal to Γ does not exist (if the wetting angle $\psi \neq 0$). In order to completely determine Γ, a smoothing of the boundary at this point is performed during the numerical procedure. According to [6], [7], if the coefficients are bounded in $\bar{G}$, the problem has a unique solution in $C^2(\bar{G} \backslash \Gamma_O)$ and (2.19'') holds on Γ_O in the integral sense. Moreover, this solution is a strictly increasing function of the boundary data T_{cr} and T_a (the maximum principle is valid for (2.20)). Here we are going to apply the numerical technique given in [9], which is based on the construction of a smoothed counterpart of (3.2) dependent on some parameter Δ_t, such that $k(T) = \lim_{\Delta_t \to 0} k(T, \Delta_t)$,

$H(T) = \lim_{\Delta_t \to 0} H(T.\Delta_t)$, where $k(T, \Delta_t)$ and $H(T, \Delta_t)$ has the form:

$$g(T, \Delta_t) = \begin{cases} g_1 & T \leq 1 - \Delta_t \\ h(T) & 1 - \Delta_t \leq T \leq 1 + \Delta_t \\ g_2 & T \geq 1 + \Delta_t \end{cases} \qquad (3.4)$$

with g_1, g_2 being constants and $h(T) \in C^{\infty}(R)$.

4. Numerical methods

In order to solve (3.2) with (3.4), (2.7')-(2.13') (the way of accounting condition (2.14') will be discussed in the next section) we shall define the current domain $\bar{G}$ by an iterative scheme.

The one-dimensional quasilinear equation of capillary statics (2.11') in terms of $H_1^* = H_1 - \gamma$:

$$\Psi_{1x} - \Psi_2 = 0, \qquad x \in [R^*, Bo^{1/2}] \qquad (4.1)$$

$$\Psi_1(x, H_1^*, H_1^{*\prime}) = \frac{xH_1^{*\prime}}{(1 + H_1^{*\prime 2})^{1/2}}$$

$$\Psi_2(x, H_1^*, H_1^{*\prime}) = xH_1^*$$

$$R^* = RBo^{1/2}$$

The boundary conditions (2.12′):

$$\Psi_1|_{x=R^*} = -R^* \cos\psi \qquad\qquad (4.2)$$

$$\Psi_1|_{x=Bo^{1/2}} = 0$$

and γ is obtained from (2.13′).

A non-linear finite-difference scheme over a non-uniform grid $\bar{\omega}=\{R^*=x_0, x_1, \ldots, x_L=Bo^{1/2}\}$ is applied to (4.1); the scheme is linearized by the simple iteration method of the implicit type, resulting in the system of equations

$$\mathcal{B}\,\frac{y_{k+1}-y_k}{\tau_c} + \mathcal{A}\,y_k = f, \quad (k=0,1,\ldots), \qquad (4.3)$$

$y_k \in \mathbb{H}(\bar{\omega}_c)$, where y_k is the grid function, τ_c is the iteration parameter, $\mathcal{B}$ and $\mathcal{A}$ are difference operators [10]. Equations (4.3) are solved by the Gaussian elimination method. Ψ_1 and Ψ_2 are continuously differentiable with respect to H_1^* and $H_1^{*'}$. The error and the iteration number estimations independent of the grid parameters are shown in [10].

The thermal problem (3.2), (3.4), (2.7′)-(2.9′) is solved numerically by a fully implicit conservative finite-difference scheme. A space grid $\bar{\omega}=\{\omega_{h^1} \times \omega_{h^2}\}$ is introduced in the region $\bar{G}$. Let the grid functions $u=\{u_{ij}\}\in\mathbb{H}(\bar{\omega})$ be defined. This stationary problem is treated as a limit of an appropriate nonstationary problem (with boundary conditions constant in time) when time tends to infinity and the method of fractional steps is used involving an implicit difference scheme for both geometrical directions:

$$\frac{\bar{u} - u^n}{0.5 \, \tau_t} = \bar{A}_1 \, \bar{u} + \bar{A}_2 \, u^n \tag{4.4}$$

$$\frac{u^{n+1} - \bar{u}}{0.5 \, \tau_t} = \bar{A}_1 \, \bar{u} + \bar{A}_2 \, u^{n+1}$$

where τ_t is a fictitious time step, $n=0,1,\ldots$ The solutions u^n converge to u in the norm $\|\blacksquare\|_{L_2}$ when $n \to \infty$. An integral-interpolation method is used in order to approximate the nonlinear operators $\bar{A}_1$ and $\bar{A}_2$ with order $O(h_{max}^2)$ and at every fictitious time step a linearization by the simple iteration method is applied [9], [11]. The iteration procedure in each of the two directions is continued till the relative difference between two successive iterations in $\|\blacksquare\|_C$ becomes of $O(h_{max}^2)$-order. Again the Gaussian elimination is applied.

Here the crystal radius R, the melt volume V_O, the crucible temperature T_{cr} and the ambient temperature T_a are assumed fixed. An outline of the solution algorithm is as follows:

1) The meniscus shape is calculated from (2.11'), (2.12');

2) The melt/crystal interface is set $H_O(r) \equiv H_1(R)$;

3) γ is defined from (2.13');

4) The height l is determined from (2.10');

5) The temperature field is calculated from (3.2), (3.4), (2.7')-(2.9');

6) The position of Γ_O is redefined as the isotherm $T=1$ and the melt region volume is recalculated. Using the former $H_O(r)$, a new $H_O(r) = H_O(r) + (H_1(R) - H_O(R))$ is set. Then return to 3) and the iterative process is continued until the melt volume $\bar{V}_O$ is achieved with an absolute error $\sim O(h_{max})$.

The idea of the algorithm consists in lifting or falling of the crucible height when the recalculated melt volume is larger or less than $\bar{V}_O$. If the crucible height is

lifted then the heat flow through the crucible walls will be
increased. In this case, because the temperature function in
the melt region is an increasing function w.r.t. T_{cr} or the
heat flow through the crucible walls, it follows that the
melt region volume will be lifted up, too. It occurs, that
the sequence of the absolute values of crucible height
changes is monotonously decreasing, which confirms the
convergence of the proposed algoritm.

5. Optimization model

As it has been shown in section 2 some of the process
parameters have to be treated as variable; with this we
shall look for a solution that satisfies (2.14'), too. Here
we restrict ourselves only to the crucible temperature T_{cr}
and ambient temperature T_a as unknowns, while the crystal
radius R, the wetting angle ψ, etc. are assumed fixed and
the change of the melt volume (or system height) corresponds
to different discrete times from the long-time scale
interval. A suitable, for practical purposes, choice of the
values of unknowns would be given by solutions of the
optimization problem including (2.14') as an additional
constraint.

We introduce a k-dimensional vector $p=(p_1,p_2,\ldots,p_k) \in$
L_2^k (Γ) as a control function with the unknown parameters as
its components, and the cost functional

$$I(p) = \| p-p^* \|^2_{L_2^k(\Gamma)} \tag{5.1}$$

where p^* is a given k-dimensional vector $\in L_2^k(\Gamma)$.

The optimization problem we are going to consider is
to minimize $I(p)$ over p, subject to $T(r,z,p)$ being solution
of (3.2), (3.4), (2.7')-(2,13') and (2.14') in the form:

$$F(p) = F_1(p) \equiv T(R,H_1(R),p) - 1 = 0 \tag{5.2}$$

Let us recall that the constraint vector function $F(p)$
consists of more than one element, if some additional
restrictions are imposed on temperature (e.g. some
distributions of temperature on the boundary or on some part

of it, some temperature gradient distributions in the domain $G\backslash\Gamma$, etc.). Of course these constraints could be added to the cost functional with appropriate weight coefficients [8].

Because p and p^* are vectors with components active on different parts of Γ (e.g. in our case $p_1=T_{cr}$ on $\Gamma^1=\Gamma_1 U \Gamma_3$, $p_2=T_a$ on $\Gamma^2=\Gamma_1 U \Gamma_4 U \Gamma_5$), on the remaining parts of Γ we shall define them as vanishing. The model can be simplified in the case where T_{cr} and p_1^* are constant on Γ^1, T_a and p_2^* are constant on Γ^2. Then (5.1) is transformed into

$$I(p) = (p_1-p_1^*)^2 \mu(\Gamma^1) + (p_2-p_2^*)^2\mu(\Gamma^2) \qquad (5.1')$$

where $\mu(\Gamma^i)$ is the Lebesgue measure of Γ^i in Γ.

We have to find a solution of the optimization problem in Σ - a k-dimensional cube $:=\{\{p\}: p \in [\underline{p}, \bar{p}]\}$, where $\underline{p}$ and $\bar{p}$ are the lower and the upper boundaries of p.

If $\Omega:=\emptyset$, where $\Omega\equiv\Omega_i\subset\Sigma : F_i=0$, then the optimization problem has no solution. If $p^*\in\Omega$, then the solution is $p=p^*$.

We are going to construct an algorithm for determining Ω, based on the dichotomic line-search using the properties of temperature distribution shown in section 3.

In case of two variable parameters the set Ω is approximated linearly by the least-squares method. The obtained line l_O, corresponding to Ω, is such that $|F(\underset{\sim}{p})|\leq\varepsilon$ on it, where ε is of order $O(h^2_{max})$. Then the solution ρ of the optimization problem exists and satisfies the relation

$-\nabla I(\underset{\sim}{\tilde{p}}) = \eta\nabla J_i(\underset{\sim}{\tilde{p}})$ at $i=0$, where η is a coefficient and
$$l_i: J_i=0. \qquad (5.3)$$

In order to follow the evolution of the constraint set as well as that of the optimal solution at different melt volumes $\bar{V}_i$ (for different discrete times from the long time scale), it turns out useful to introduce the parametrization

$$l_i: \{p=p^O + s\vec{t} + f(\bar{V}_O- \bar{V}_i)\vec{n}\}, \quad i=0,1,\ldots \qquad (5.4)$$

where $s \in R$, $f(\bar{V}_O- \bar{V}_i)$ is a function of $(\bar{V}_O-\bar{V}_i)$, $\vec{t}$ and $\vec{n}$

are the unit tangent and normal vectors to l_O, respectively.
The representation (5.4) describes a one-parameter family of
parallel lines and it turns out convenient to take $f(\bar{V}_O - \bar{V}_i)$
linear:

$$f(\bar{V}_O - \bar{V}_i) = a_1(\bar{V}_O - \bar{V}_i) \quad \text{with } a_1 = \text{const.} \tag{5.5}$$

6. Numerical results and discussion

Based on the algorithms given in sections 4-5, a
computer realization was implemented on IBM PC-AT.
Calculations were performed for two semiconductor materials:
Ge and GaAs.

All the physical and geometrical parameters for the
two materials are given in the Appendix. The geometrical
mesh sizes are $h_{min} \sim 5.10^{-4}$, $h_{max} \sim 10^{-3}$ and the remaining
parameters are: $\tau_t \sim 0(h_{min})$, $\tau_c \sim 10^{-1}$, $L \sim 0(10^2)$, $\varepsilon \sim 10^{-3}$,
$\Delta_t \sim 10^{-3}$.

In the GaAs and Ge cases, the crystal radius is fixed
- $R = 0.75$ and $\bar{V}_O = 1$, $\bar{V}_1 = 0.5$ and $\bar{V}_2 = 0.3$ are taken as $\bar{V}_i$, and
$p_1 = 1.01$, $\bar{p}_1 = 1.1$, $p_2 = 0.85$, $\bar{p}_2 = 0.99$-as parameters boundaries.
In Fig.2 and Fig 4 the line of approximated constraint l_O
and its propagation due to (5.4) are shown for both cases.
If for GaAs and Ge case p^* are constant for different $\bar{V}_i$ and
have the corresponding values $p^* = (1.067, 0.954)$, $p^* = (1.04,
0.954)$, then the optimal solutions are $\tilde{p}(\bar{V}_O) = (1.048, 0.94)$
and $\tilde{p}(\bar{V}_O) = (1.018, 0.95)$. From the parametrization (5.4)
the solutions for different $\bar{V}_i$ are $\tilde{p}(\bar{V}_1) = (1.039, 0.933)$,
$\tilde{p} \bar{V}_2) = (1.035, 0.93)$ in the first case and $\tilde{p}(\bar{V}_2) = (1.013, 0.949)$,
$\tilde{p}(\bar{V}_2) = (1.01, 0.948)$ in the second case.

These points are marked with asterisks and the isotherms
related to them are plotted (Fig. 3a,b,c and Fig.
5a,b,c.).The isotherms are incremented by $11^O K$.

The above results are derived for the propagation (5.4) approximated by a family of parallel lines $a_1 = 0,024$, $\vec{n} = (-0.803, -0.596)$ (for the GaAs case) and $a_1 = 0,011$, $\vec{n} = (-0.979, -0.202)$ (for the Ge case).
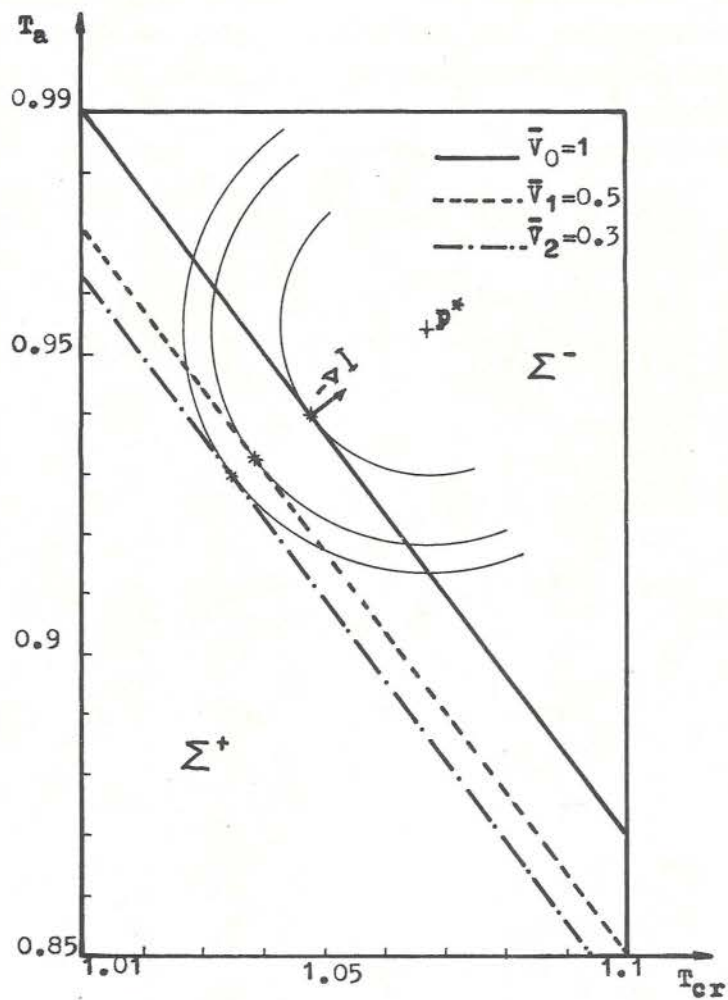
Fig. 2. Constraint set and optimal solution propagation for $\bar{V}_i$, $i = 0,1,2$ in the GaAs case

The numerical experiments performed for other values of the crystal radius show that the space in the cube Σ_{GaAs} and in Σ_{Ge} is decomposed into two half-spaces: Σ^+ and Σ^- corresponding to such $p \in \Sigma$ for which the temperature is calculated at ($R > 0.75$, $\bar{V}_O = 1$) or ($R = 0.75$, $\bar{V}_O < 1$) and at ($R < 0.75$, $\bar{V}_O = 1$) or ($R = 0.75$, $\bar{V}_O > 1$), respectively (Fig.2, Fig.4). The difference between the two materials (GaAs and Ge) is evident - the lower conductivity of GaAs leads to higher Bi and Ra and this explains the GaAs tendency to create thicker crystals. This tendency is confirmed by the results obtained in [3], [4] using finite element techniques.
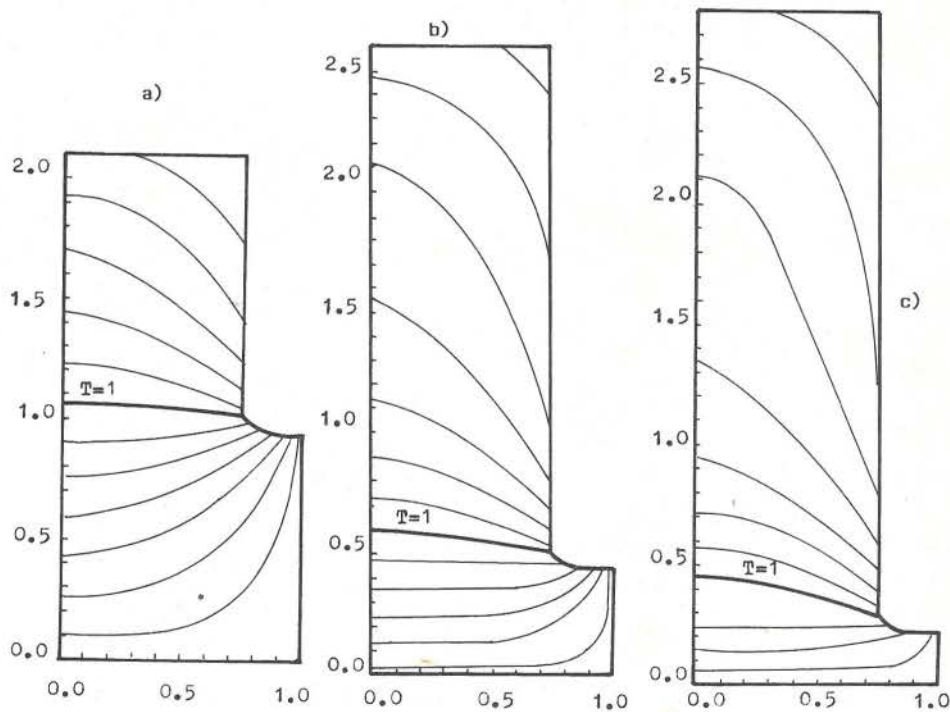
Fig. 3. Temperature distribution of the optimal solution
        points for the GaAs case
        a) $Tcr = 1.048$, $Ta = 0.94$, $R = 0.75$, $\bar{V}_O = 1$

b) Tcr=1.039, Ta=0.933, R=0.75, $\bar{V}_1$=0.5

c) Tcr=1.035, Ta=0.93, R=0.75, $\bar{V}_2$=0.3

The optimal propagation model based on the solution of the stationary Stefan problem for discrete times over fixed domain which we have considered, yields prediction of the temperature distribution as well as contributes to constant-radius control through discrete changes of the melt volume. This model could be used as a starting point to a more comprehensive one, including convection, some improvements on the boundary conditions that correspond to a more realistic technological situation, impurities distribution, surface tension on the phase change boundary, etc.
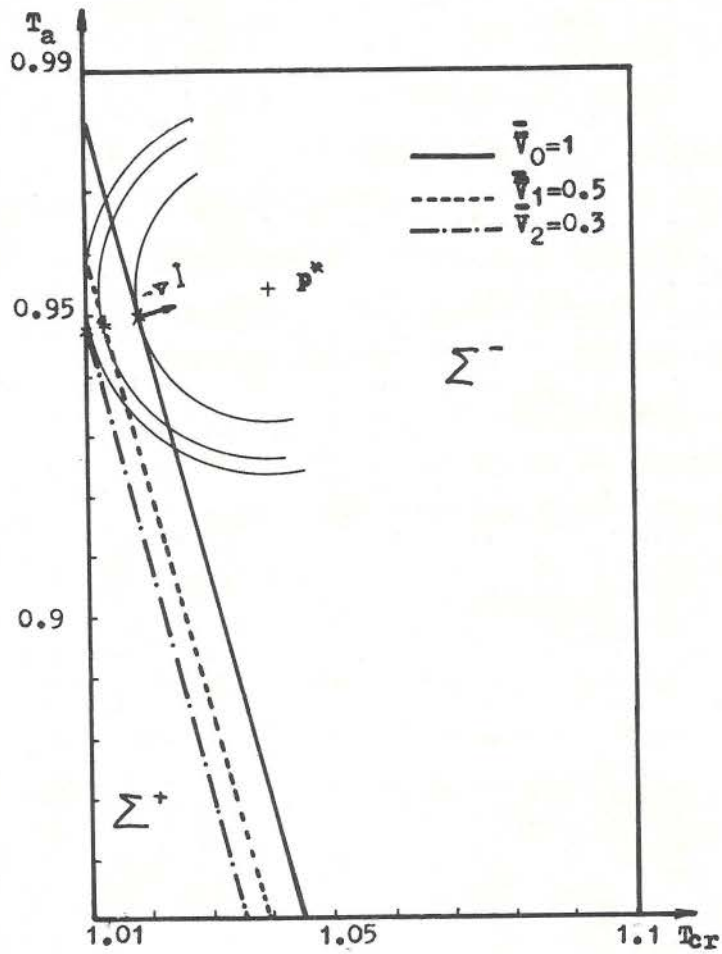
Fig.4. Constraint set and optimal solution propagation for

$\bar{V}_i$, $i=0,1,2$ in the Ge case
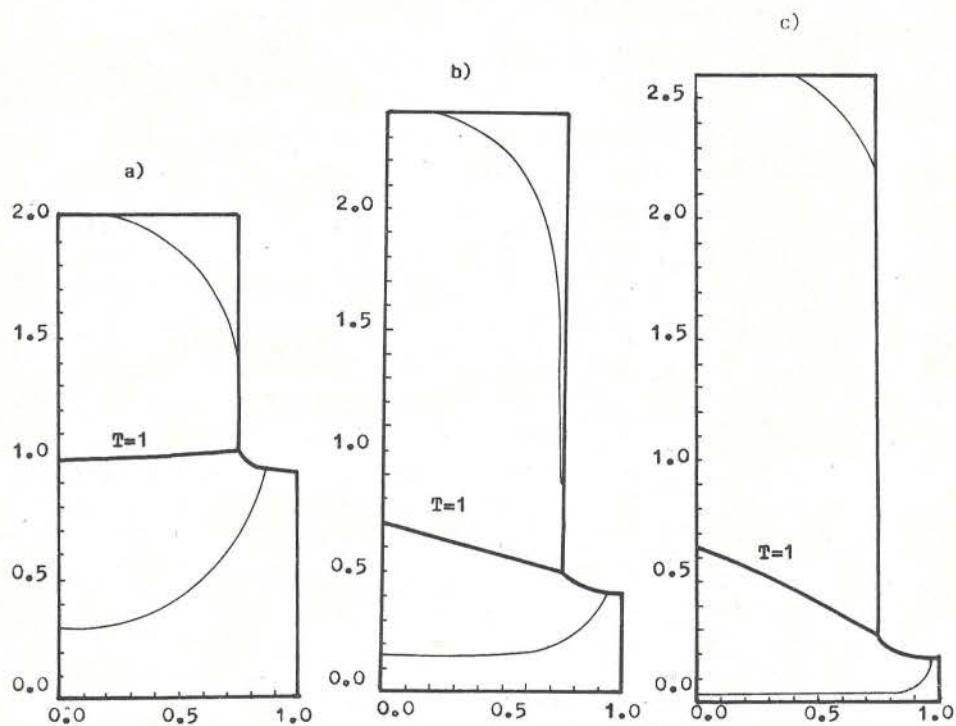
Fig.5. Temperature distribution of the optimal solution
      points for the Ge case
        a) Tcr=1.018, Ta=0.95, R=0.75, $\bar{V}_O$=1
        b) Tcr=1.013, Ta=0.949, R=0.75, $\bar{V}_1$=0.5
        c) Tcr=1.01, Ta=0.948, R=0.75, $\bar{V}_2$=0.3

Appendix

	Basic notations		*Used values*

a — crucible radius [cm]   =5 cm

$Bi_j \equiv \alpha_j a / \lambda_1$ — Biot number for Γ_j =0.025(GaAs);0.0042(Ge)

$Bo \equiv g \rho_1 a^2 / \sigma_m$ — Bond number   =370(GaAs);225(Ge)

c_{pi} — heat capacity [$J/g\ ^\circ K$]

$e_r,\ e_z$ — unit coordinate vectors

g — gravitational constant [cm/sec^2]

$h^1,\ h^2$ — grid steps in $r,\ z$ direction

H_f — heat of fusion [J/g]

k_i — thermal conductivity k_2=0.5(GaAs);0.338(Ge)

ratio k_1=1

M_O — total mass [g]   =3468(GaAs);3340(Ge)

$\hat{p}'$ — pressure [$g/$cm sec^2]

$Pe_p S$ =0.1(GaAs,Ge)

R — dimensionless crystal radius

$Ra_j \equiv \sigma \varepsilon_j a \theta_m^3 / \lambda_i$ — radiation number for Γ_j =0.4(GaAs);0.14147(Ge)

t — time [sec]

T — dimensionless temperature

U — velocity vector

U_p — crystal pull rate [cm/sec]

V — dimensionless velocity vector

$\bar{V}_O$ — dimensionless melt volume

V_O — melt volume [cm^3]

α_j — heat transfer coefficient for Γ_j [$W/$cm$^2\ ^\circ K$]

β — volume expansion coefficient [$1/deg$]

$\varkappa_i$ — principal curvature radii

λ_i — thermal conductivity [$W/$cm $^\circ K$]

ν — melt viscosity [cm$^2/$sec]

ρ_i — density [$g/$cm^3]

σ_m — melt surface tension [dyn/cm]

σ — Stefan-Boltzmann constant [$W/$cm$^2\ ^\circ K^4$]

ε_j — emissivity of surface Γ_j

Θ - temperature $[^{\circ}K]$

Θ_a - ambient temperature $[^{\circ}K]$

Θ_{cr} - crucible temperature $[^{\circ}K]$

Θ_m - melting temperature $[^{\circ}K]$ $=1511^{\circ}K(GaAs);1210^{\circ}K(Ge)$

ψ - equilibrium wetting angle = $15^{\circ}(GaAs);\ 8^{\circ}(Ge)$

τ - dimensionless time

References

[1] CROWLEY A.B. On the weak solution of moving boundary problems. *J.Inst. Math. Applic.*, **24** (1979),43-57.

[2] CROWLEY A.B. Mathematical modelling of heat flow in Czochralski crystal pulling. *IMA J.Appl.Math.* **30** (1983), 173-189.

[3] DERBY J.J., BROWN R.A. Thermal-capillary analysis of the Czochralski and liquid encapsulated Czochralski crystal growth. I.Simulation. *J.Crystal Growth* **74** (1986), 605-624.

[4] DERBY J.J., BROWN R.A. Thermal-capillary analysis of the Czochralski and liquid encapsulated Czochralski crystal growth. II.Processing strategies. *J.Crystal Growth* **75** (1986), 227-240.

[5] МЕЙРМАНОВ А.М. .Задача Стефана. Новосибирск, Наука 1986.

[6] ОЛЕЙНИК О.А., КРУЧКОВ С.Н. О некоторых нелинейных задачах для уравнений эллиптического типа. УСПЕХИ МАТ. НАУК,Т.XV, вып.5 (1960), 203-206.

[7] ОЛЕЙНИК О.А. Об одном методе решения обшчей задачи Стефана. ДОКЛАДЫ АН СССР, Т.**135**, вып.5 (1960), 1054 - 1057.

[8] PAWŁOW I. Analysis and control in free boundary problems. *Bulletin of the Faculty of Education,* Chiba Univ. **36**, Feb. 1988.

[9] САМАРСКИЙ А.А., МОИСЕЕНКО Б.Д. Економичная схема сквозного счета для многомерной задачи Стефана. ЖВММФ **5** (1965), 816-827.

[10] САМАРСКИЙ А.А., НИКОЛАЕВ Е.С. Методы решения сеточных уравнехий. Москва, Наука 1978.

[11] TABACOVA S.S. Finite-difference numerical analysis of the thermal-capillary two-dimensional Czochralski crystal growth. *Theor. and Appl. Mechanics*, **19** (1988), No.1, 70-80

O DWUWYMIAROWYM MODELOWANIU NUMERYCZNYM PROCESÓW TECHNICZ-
NYCH W PROCESIE WZROSTU KRYSZTAŁU CZOCHRALSKIEGO ZE STOPIO-
NEJ MASY

W pracy przedstawiono dwuwymiarowy stacjonarny model
matematyczny, oparty przede wszystkim na przewodzeniu
ciepła: procesów cieplno-kapilarnych wzrostu kryształu
Czochralskiego. Na podstawie tego modelu sformułowano
zadanie optymalizacji. Temperatury: naczynia i otoczenia są
używane jako parametry sterujące. Funkcjonał kosztu zależny
od wektora sterowań ma postać kwadratową. Warunek stałego
promieniowania kryształu stanowi dodatkowe ograniczenie.
Wyznaczono·rozwiązanie optymalne i warunki ograniczeń dla
różnych dyskretnych objętości stopionej masy. Eksperymenty
numeryczne zostały przeprowadzone dla dwóch różnych
materiałów półprzewodnikowych.

О ДВУХМЕРНОМ ЧИСЛЕННОМ МОДЕЛИРОВАНИИ ТЕХНИЧЕСКИХ ПРОЦЕССОВ
В ПРОЦЕССЕ РОСТА КРИСТАЛЛА ЧОХРАЛЬСКОГО ИЗ ПЛАВЯЩЕЙСЯ МАССЫ

В работе представлена двухмерная стационарная
математическая модель, основанная на теплопроводимости:
тепло-капилярных процессов роста кристалла Чохральского. На
основе этой модели формулируется задача оптимизации.
Температуры: сосуда и окружающей среды используются в
качестве параметров управления. Функционал затрат,
зависящий от вектора управлений имеет квадратный
вид. Условие постоянного радиуса кристалла является
дополнительным ограничением для разных дискретных объемов
плавящейся массы. Численные эксперименты проводилсъ для
двух разных полупроводниковых материалов.